

Evolution of coherent islands in $\text{Si}_{1-x}\text{Ge}_x/\text{Si}(001)$

J. A. Floro and E. Chason

Sandia National Laboratories, Albuquerque, New Mexico 87185-1415

L. B. Freund

Division of Engineering, Brown University, Providence, Rhode Island 02912

R. D. Twisten

Center for Microanalysis of Materials, University of Illinois, Urbana, Illinois 61801-2985

R. Q. Hwang

Sandia National Laboratories, Livermore, California 94551

G. A. Lucadamo

Department of Materials Science and Engineering, Lehigh University, Bethlehem, Pennsylvania

(Received 31 August 1998)

The evolution of strain driven coherent islands is examined using sensitive real time stress measurements during heteroepitaxial growth of $\text{Si}_{1-x}\text{Ge}_x/\text{Si}(001)$, combined with *ex situ* microscopy. We show that the sequence of morphological transitions at low mismatch strain is qualitatively identical to that for pure Ge heteroepitaxy on Si(001). In particular, films with strains less than 1% undergo Stranski-Krastanov-like island-on-layer growth, followed by an extended regime of [501]-faceted hut clusters that eventually transform into higher aspect ratio dome clusters. The hut and dome islands are fully coherently strained and do not exhibit lateral composition modulation. Quantitatively, the relevant island length scales are significantly increased at low strain. Scaling of the morphological transitions with strain is directly demonstrated using the real time stress data. We further show that the apparent formation of a ripplelike surface morphology at low strain is actually a consequence of kinetic limitations on adatom diffusion, and does not necessarily signify the presence of a surface instability. [S0163-1829(99)01704-X]

INTRODUCTION

The large strains often associated with lattice mismatched heteroepitaxy provide a significant reservoir of elastic energy that can be released to drive structural and morphological evolution of the growing film. Under deposition conditions favoring high surface mobility, strain relaxation via three-dimensional (3D) surface roughening can precede the conventional mode of strain relaxation via dislocation formation. The 2D-to-3D transition reduces the elastic energy through geometry, since lateral constraints are partially relaxed in regions of the film where the free surface is inclined to the interface. At high mismatch the surface roughness takes the form of isolated islands.¹⁻⁴ At lower mismatch, it has been observed that roughening may occur in the form of a continuous surface ripple that does not reach the film/substrate interface;⁵ this has been attributed to a strain driven surface instability of the type suggested by Asaro and Tiller,⁶ Grinfeld,⁷ and others.^{8,9} It is one of the goals of this work to determine if there is a fundamental difference between these observations, or whether they are manifestations of the same effect.

Although there is much interest in exploiting strain driven islanding for the formation of nanostructures exhibiting quantum confinement for optoelectronic devices, precise manipulation of the growth process is required to produce highly monodisperse island arrays. So far, however, many

aspects of coherent island formation and evolution remain poorly understood. In this article we report on the detailed evolution of coherent island arrays during $\text{Si}_{1-x}\text{Ge}_x$ molecular beam epitaxy (MBE) on Si(001). We obtain real time measurements of the evolution of film stress during the deposition process. Supplemented by extensive *ex situ* imaging, the stress measurement provides quantitative information on the dynamic islanding process that would be difficult to obtain iteratively.

The primary purpose of this article is to demonstrate that strain driven roughening behavior at relatively low mismatch strain (0.8–1.4%) is qualitatively identical to that at much higher strains. In particular, dilute alloys are shown to undergo exactly the same sequence of islanding transitions as are observed for epitaxial growth of Ge on Si(001), where the mismatch strain is 4%. In order to observe this behavior in the low strain regime, however, the deposition temperature must be high enough to allow adatom migration to access length scales that can be more than an order of magnitude larger than in the case of Ge/Si. Longer length scales are a consequence of the nature of strain driven islanding, where surface energy acts as an energetic barrier against island formation. This imposes a length scale proportional to $\Delta\Gamma/M\varepsilon_{\text{coh}}^2$, where $\Delta\Gamma$ is the increase in surface energy due to island formation, ε_{coh} is the lattice mismatch (or coherency) strain, and M is an elastic modulus. Here we will directly demonstrate the increase in length scale with decreasing

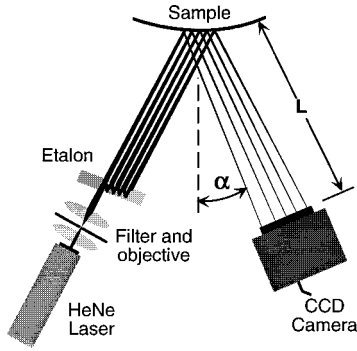


FIG. 1. Schematic illustration of the MOSS setup.

ing strain. We also show that at lower deposition temperature, the apparent formation of continuous ripples rather than discrete islands is not a fundamentally different roughening phenomenon (e.g., a surface instability), but is instead simply due to kinetic constraints imposed upon the islanding process.

EXPERIMENTAL

Film deposition

$\text{Si}_{1-x}\text{Ge}_x$ films were grown by molecular-beam epitaxy (MBE) electron-beam evaporation in an ultrahigh vacuum chamber with a base pressure of 1×10^{-10} Torr. The deposition rates of Si and Ge were independently controlled by quartz-crystal monitors that were calibrated by *ex situ* x-ray measurements of film thickness and composition. Si(001) substrates (100 μm thick) were prepared by *ex situ* chemical cleaning. The nonstoichiometric oxide produced in the final step of the chemical cleaning was desorbed *in situ* at 830 $^\circ\text{C}$ and a 1000–1200 \AA Si buffer was then grown at 750 $^\circ\text{C}$. The reflection high-energy electron diffraction (RHEED) pattern obtained following the buffer consisted of a Laue circle of sharp spots characteristic of the 2×1 reconstruction. The RHEED pattern, acquired along either the $\langle 110 \rangle$ or $\langle 100 \rangle$ azimuth in the out-of-phase condition, was recorded on videotape during deposition. The deposition rate Φ was 0.1 $\text{\AA}/\text{s}$. Concurrently with RHEED, the film stress was measured in real time. This measurement is described in the next section. After deposition, the films were analyzed *ex situ* using scanning electron microscopy (SEM), atomic force microscopy (AFM), and/or transmission electron microscopy (TEM).

Real time stress measurement

The evolving film stress due to coherent island formation is obtained in real time during deposition through measurement of the substrate curvature using an apparatus called the multi-beam optical stress sensor (MOSS).^{10,11} A schematic illustration of the technique is shown in Fig. 1. Briefly, a HeNe laser beam passes through a highly reflective etalon that produces a linear array of parallel output beams. The beam array reflects off the sample (which is mounted in such a way that it is fully free to bend) and is then detected on a charge-coupled device (CCD) camera. The distance between adjacent laser spots, $D(t)$, is recorded during deposition. Changes in substrate curvature due to an evolving film stress

produce changes in the angular divergence of the beam array, and therefore the spacing of the laser spots on the CCD. The substrate curvature, $\kappa(t)$, is determined as

$$\kappa(t) = \frac{\cos(\alpha)}{2L} \left(1 - \left\langle \frac{D(t)}{D_0} \right\rangle \right), \quad (1)$$

where $\langle D(t)/D_0 \rangle$ is the spacing between adjacent beams, normalized by the initial spacing (averaged over all beams), L is the sample-to-CCD distance, and α is the angle of incidence, as shown in Fig. 1. The MOSS technique is operationally simple, and demonstrates reduced sensitivity to ambient vibration compared with serial scanning deflectometers.¹² Further details may be found in the references.^{10,11}

The substrate curvature is related to the lattice mismatch stress σ_{coh} , and the surface stress, ΔF ,¹³ by Stoney's equation^{14,12}

$$\kappa(t) = \frac{6[\sigma_{\text{coh}}(t)h_f(t) + \Delta F(t)]}{M_s h_s^2}, \quad (2)$$

where h_f (h_s) is the film (substrate) thickness, and M_s is the substrate biaxial modulus. Substrate curvature is, therefore, proportional to the product of the film stress and the film thickness, which we will call the stress-thickness S . In order to obtain the stress, $h_f(t)$ must be known independently. For the 100 μm -thick Si wafers used in these experiments, our sensitivity is about 0.5 GPa \AA , i.e., a 0.5- \AA -thick film with 1 GPa stress can be detected by MOSS. For a film with non-uniform thickness, e.g., due to island formation, the curvature measurement provides an effective stress at the mass equivalent thickness h_f .

We have also simultaneously measured, in real time, the spatial period and coherence length of the island array using a technique called light scattering spectroscopy (LiSSp).¹⁵ Results of those measurements are discussed elsewhere.^{16,17}

ROUGHENING TRANSITIONS

We show in what follows that the evolution of the surface morphology during MBE growth of $\text{Si}_{1-x}\text{Ge}_x/\text{Si}(001)$ can be broken into four regimes: two-dimensional growth and roughening, three-dimensional nucleation, hut cluster formation, and dome cluster formation. The transitions can be determined from the real time stress data as discussed below.

2D growth and roughening

Figure 2(a) shows the stress-thickness S vs deposited thickness h_f obtained using MOSS during MBE growth of $\text{Si}_{0.8}\text{Ge}_{0.2}/\text{Si}(001)$ at 755 $^\circ\text{C}$.¹⁸ The slope dS/dh is the instantaneous effective stress of the film. This is plotted in Fig. 2(b), where filtering to remove high-frequency noise has been applied prior to numerical differentiation. The line through the data in Fig. 2(b) is a guide to the eye. For a coherently strained, planar film grown at constant deposition rate S vs h_f will be linear since the stress is constant and h_f increases linearly with time. This behavior is observed for low-temperature deposition of $\text{Si}_{1-x}\text{Ge}_x/\text{Si}$, where both dislocation introduction and surface roughening are suppressed.^{10,11} The initial nonlinear regime observed in Fig.

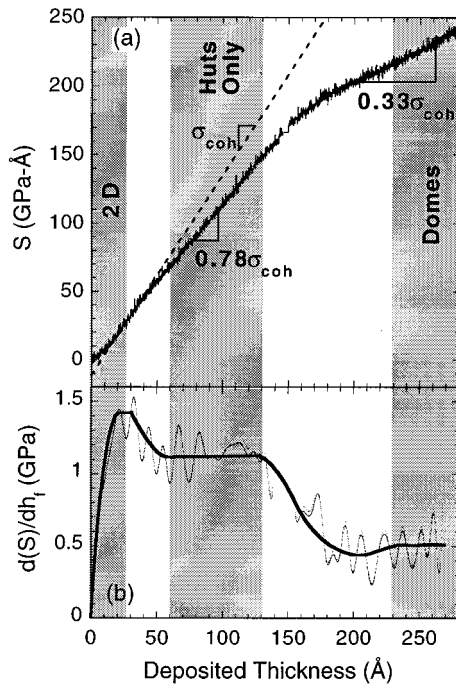


FIG. 2. (a) Stress thickness (S) vs deposited film thickness h_f , measured by MOSS during MBE growth of $\text{Si}_{0.8}\text{Ge}_{0.2}/\text{Si}(001)$ at 755°C . (b) Instantaneous stress vs deposited film thickness, obtained by smoothing and differentiation of the data in (a). The heavy line is a guide to the eye.

2(a) for the first 12 \AA of deposition arises from Ge surface segregation.¹⁹ From $h_f=12\text{--}25\text{ \AA}$, $S(h_f)$ is linear, with a least-squares fit to the slope of the dashed line in Fig. 2(a) yielding a coherency stress of $1.4\pm 0.2\text{ GPa}$, close to the value of 1.38 GPa expected for $\text{Si}_{0.8}\text{Ge}_{0.2}$. RHEED indicates that the film grows in step flow for the first 12 \AA [see Fig. 3(a)]. From $h_f=12\text{--}25\text{ \AA}$, RHEED shows that while the film continues to grow in a layer-by-layer mode, the diffraction spots extend into streaks and the half order spot intensity quenches, both of which indicate that the step density is rapidly increasing [see Figs. 3(b) and 3(c)]. This stress driven increase in the 2D island density serves as a precursor to 3D island formation.^{20,21} The region from $0\text{--}25\text{ \AA}$ is labeled as the “2D” regime in Fig. 2.

3D nucleation

From $25\text{--}65\text{ \AA}$ deposited film thickness, the measured stress-thickness curve exhibits a slope transition region in which stress relaxation is occurring. Note that the equilibrium critical thickness (the “Matthews-Blakeslee” critical thickness²²) for the introduction of misfit dislocations is 100 \AA . An AFM micrograph of the surface morphology at $h_f=25\text{ \AA}$ is shown in Fig. 4(a). Small, discrete islands are observed to be forming, but the rms roughness is still only 6 \AA , i.e., the film is still essentially flat. This is supported by RHEED, which still exhibits a streaky pattern, corresponding to 2D roughness. We note that the islands are clearly not laterally ordered on the surface, and cooperative nucleation is not observed.²³ Shortly after this nucleation of a very low areal density of apparently discrete islands, the density increases rapidly. At 35 \AA thickness, the surface develops a

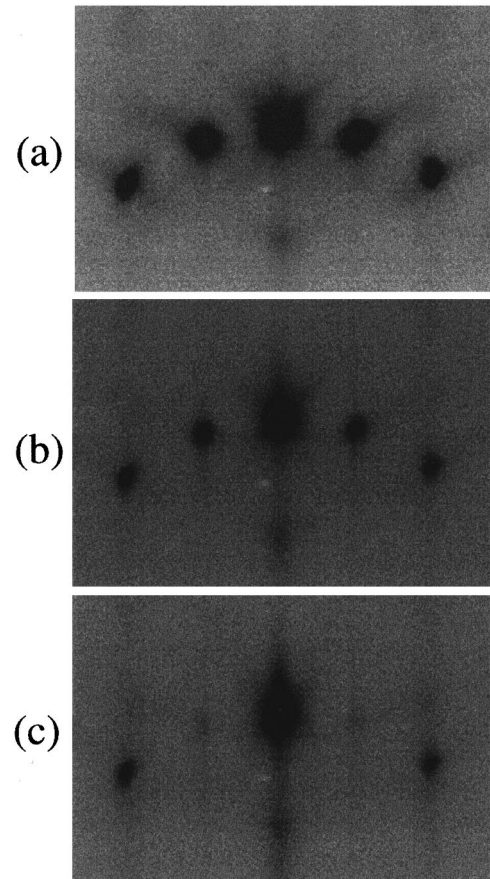


FIG. 3. RHEED patterns obtained at (a) 10 \AA , (b) 17 \AA , and (c) 25 \AA deposited film thickness.

more interconnected island array that appears somewhat ripplelike, as shown in Fig. 4(b). The angle between the sides of the islands and the substrate is in the range $1\text{--}3^\circ$.

The hut cluster regime

Subsequent to the nucleation regime, the stress-thickness evolves with a constant slope of $1.15\pm 0.06\text{ GPa}$. Figure 5(a) shows the morphology in this regime. The surface is populated with an array of discrete pyramidal islands bound by $[501]$ facets as measured from AFM height profiles. These are just a compact, i.e., square based form of the now well-known “hut cluster” first observed by Mo *et al.* in Ge/Si(001) MBE growth.¹ The mean base length of the $\text{Si}_{0.8}\text{Ge}_{0.2}$ huts is 3300 \AA , compared with only 200 \AA for the Ge huts observed by Mo *et al.* Plan view TEM shows that the $\text{Si}_{0.8}\text{Ge}_{0.2}$ huts are fully coherent. The SEM image in Fig. 5(a) indicates that the huts locally order on a square mesh along the $\langle 100 \rangle$ directions.

We grew a sample 65 \AA thick, to coincide with the end of the nucleation regime, and capped the sample *in situ* with amorphous Si to prevent oxidation. XTEM of this sample resolves the presence of a $20\text{--}30\text{-\AA}$ -thick planar alloy wetting layer below and between the hut clusters.¹⁸ This thickness corresponds to the deposited thickness at the beginning of the islanding transition, which suggests that the film grows 2D for $\approx 25\text{ \AA}$ (18 monolayers), and then all material subsequently deposited clusters into 3D islands on top of this relatively thick wetting layer. This is similar to hetero-

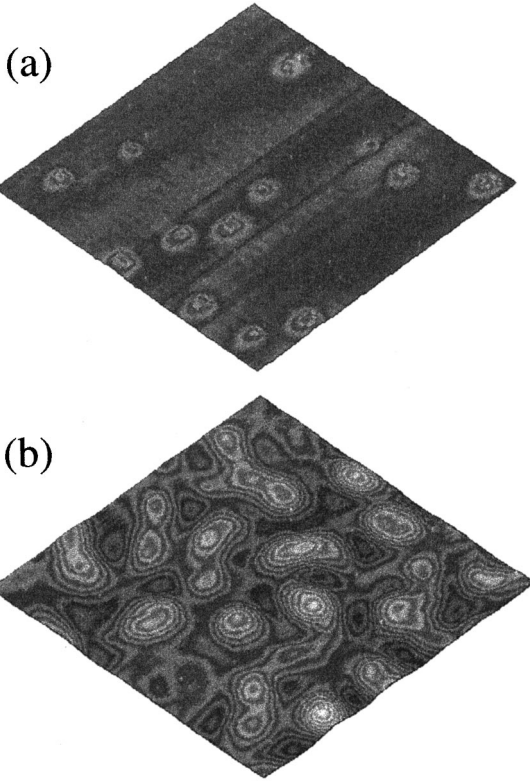


FIG. 4. $2 \times 2 \mu\text{m}$ AFM images of film at (a) 25 Å and (b) 35 Å deposited thickness.

epitaxy of pure Ge on Si(001), which grows in the Stranski-Krastanov (SK) mode, but with a wetting layer thickness of only 3 ml.^{1,24,25}

The linear $S(h_f)$ behavior from 65–130 Å in Fig. 2(a) is consistent with the growth of islands that have constant shape. Specifically, the curvature evolution during coherent islanding, including the presence of a planar wetting layer beneath the islands, is given by

$$\kappa(t) \langle \sigma_{\text{eff}} \rangle \Phi t = \sigma_{\text{coh}} h_w(t) + \langle \sigma_{\text{isl}} \rangle [\Phi t - h_w(t)], \quad (3)$$

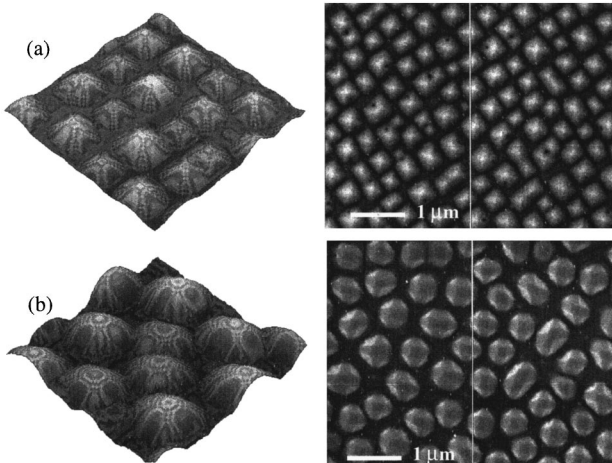


FIG. 5. AFM and SEM images from (a) hut cluster array at $h_f = 104 \text{ Å}$ and (b) dome clusters at $h_f = 275 \text{ Å}$. AFM images are $2 \times 2 \mu\text{m}$.

where $\langle \sigma_{\text{eff}} \rangle$ is the instantaneous effective stress, i.e., the uniform stress in a planar film having the same deposited thickness that would produce a curvature $\kappa(t)$. σ_{coh} is the coherency stress due to the lattice mismatch, $\langle \sigma_{\text{isl}} \rangle$ is the effective stress of the coherent island array, h_w is the thickness of the wetting layer, and Φ is the deposition rate. Changes in surface stress do not contribute significantly in this regime, and are ignored here.¹⁸ Assuming the islands all have the same shape, but not necessarily size, at any given film thickness, the effective island stress can be written as

$$\langle \sigma_{\text{isl}} \rangle = g[\mathcal{A}(t)] \sigma_{\text{coh}}, \quad (4)$$

where $g[\mathcal{A}(t)]$ is the fractional stress relaxation of an island with aspect ratio \mathcal{A} (we define \mathcal{A} as the ratio of the full island height to the full island width). According to Eqs. (3) and (4), our observation of linear curvature evolution from 65–130 Å means that $g(\mathcal{A})$ is constant, i.e., that the island shape is not changing with time.²⁶ AFM, SEM, and XTEM measurements of films grown with thickness from 65–130 Å also support this conclusion. We thus label this region as the “huts only” regime.

The linear curvature evolution also suggests that the wetting layer thickness must be constant or at least varying slowly relative to the deposition rate. XTEM measurements suggest that the wetting layer is slowly consumed during deposition above 65 Å total thickness, although the rate of consumption has not been determined. From the slope of our curvature data, and using Eq. (1), we find that hut clusters relax $20 \pm 2\%$ of the effective stress in the film [$g(\mathcal{A}) = 0.8 \pm 0.02$], where the uncertainty arises from uncertainty in the measurement of the wetting layer thickness as a function of film thickness. This degree of relaxation for hut clusters is consistent with results of 2D finite element calculations performed for islands configured as isosceles triangles with a facet angle of 11.3° (the angle between [501] and [001]).²⁷

The dome transition

In the film thickness range $h_f = 130\text{--}210 \text{ Å}$, another reduction in the effective stress is observed (see Fig. 3). After this transition, we find that the islands have changed shape, as shown in Fig. 5(b). These islands, which we will call dome clusters after Tomitori *et al.*²⁵ appear isotropic in shape, but are actually composed of several different facet types, primarily [201] and [311].²⁸ The increased aspect ratio of this island relative to the hut clusters further relaxes the overall stress, although presumably at the cost of increased surface energy.^{16,18,29} The instantaneous effective stress in the dome regime is $0.45 \pm 0.03 \text{ GPa}$, which is only 33% of the coherency stress, and the film is still free of dislocations according to plan view TEM. The areal coverage of domes (defined here as the fraction of the substrate surface covered by islands) at 275 Å film thickness is actually less than that of huts at 104 Å thickness (see Fig. 5). This transition yields significant insights into the effect of elastic repulsion between islands on both the energetics and kinetics of the evolving morphology. The hut-to-dome transition is discussed in detail elsewhere.¹⁶

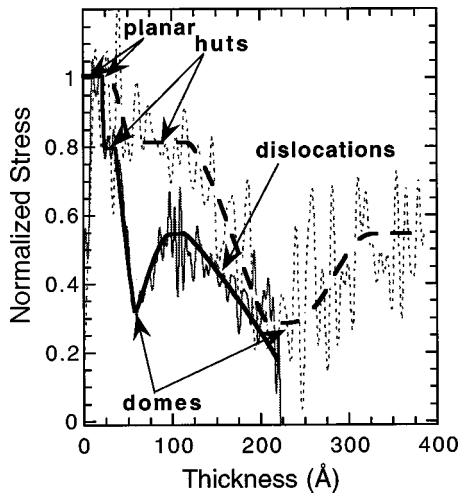


FIG. 6. Instantaneous stresses during MBE growth of $\text{Si}_{0.65}\text{Ge}_{0.35}$ (solid line) at 678 °C and $\text{Si}_{0.8}\text{Ge}_{0.2}$ at 755 °C (dotted line). The heavy lines are guides to the eye.

STRAIN SCALING

In this section we explicitly demonstrate the effect of the magnitude of the coherency strain on the roughening transitions. Figure 6 compares the stress evolution during MBE growth of $\text{Si}_{0.8}\text{Ge}_{0.2}$ and $\text{Si}_{0.65}\text{Ge}_{0.35}$ on Si(001). The same sequence of roughening transitions is observed in both cases, but the transitions at higher strain occur at smaller thicknesses (despite the fact that the 20% Ge film was grown at 755 °C, while the 35% Ge film was grown at 685 °C). The instantaneous stresses in the hut and dome regimes are nearly identical in both films. Subsequent to the dome regime, the instantaneous stress actually increases in both films. This arises from impingement of dome clusters as the areal coverage approaches unity, whereupon the overlapping elastic fields in the substrate increase the strain energy and force the clusters to change shape. This energetically unfavorable situation is observed only because of kinetic constraints imposed during deposition. For the $\text{Si}_{0.65}\text{Ge}_{0.35}$ film, another decrease in stress is eventually observed at 115 Å thickness. This results when misfit dislocations finally begin to enter the islands, as shown in Fig. 7. The dislocated islands are larger than the coherent islands, since the lower total energy of the dislocated islands increases their local growth rate.^{24,30} For the $\text{Si}_{0.8}\text{Ge}_{0.2}$ film, even though the deposition temperature is higher, plasticity does not occur up to 400 Å total film thickness, due to the lower mismatch strain.

KINETIC LIMITATIONS

In Fig. 8 we show the effect of reducing the deposition temperature for growth of $\text{Si}_{0.8}\text{Ge}_{0.2}/\text{Si}(001)$. The real time MOSS data shows that 3D roughening occurs at larger film thickness, and that the overall degree of stress relaxation is less, for 630 °C deposition versus deposition at 755 °C (compare with Fig. 2). At 630 °C, 3D roughening begins at 60 Å film thickness, followed by a minimum in the instantaneous stress at 130 Å. The instantaneous stress then increases, and finally an extended regime of linear curvature evolution (constant stress) is observed from 180–400 Å. The linear region is similar to the behavior observed in the huts only

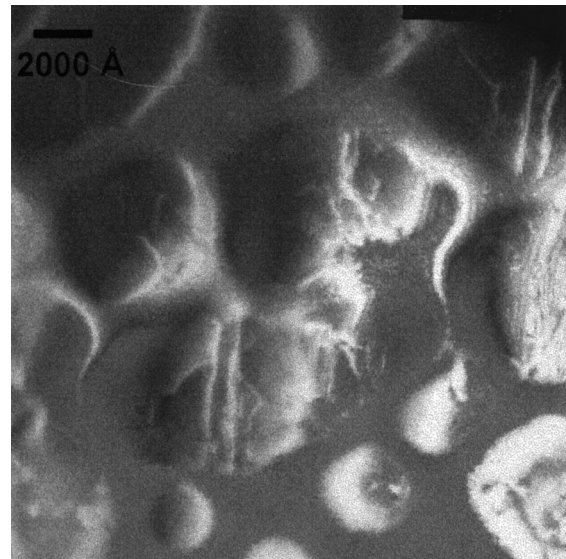


FIG. 7. Plan view TEM image of a 400 Å $\text{Si}_{0.65}\text{Ge}_{0.35}$ film deposited at 678 °C showing dislocations in the larger islands.

regime in Fig. 2, except that the steady-state stress relaxation at 630 °C is only 10% (i.e., $\langle\sigma_{\text{eff}}\rangle=0.9\sigma_{\text{coh}}$).

Figure 9 reveals two contributions to the reduced stress relaxation at 630 °C vs 755 °C. AFM [Fig. 9(a)] of a 400 Å film deposited at 630 °C show that the film surface consists of a set of interconnected ridges along the $\langle 100 \rangle$ directions, rather than discrete islands. The ridges, which are composed of $[501]$ facets, average about two times longer than they are wide, and therefore are less efficient at relieving strain compared to compact hut clusters.

In addition, Fig. 9(b) shows a cross-section TEM micrograph of the 400-Å-thick film. The film in cross section appears to exhibit a ripplelike morphology. A continuous wetting layer of approximately 200 Å thickness is clearly observed beneath the ripple. Note from Eq. (3) that if the wetting layer *grows* during deposition, in competition with the island layer, then the fractional degree of stress relaxation for the film as a whole will be reduced, as we observe. The

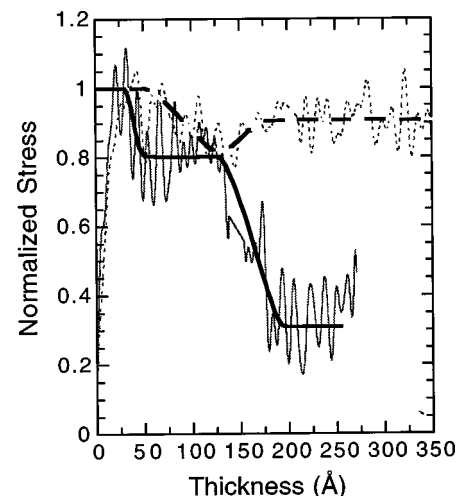


FIG. 8. Instantaneous stresses during MBE growth of $\text{Si}_{0.8}\text{Ge}_{0.2}$ at 755 °C (solid line) and 630 °C (dotted line). The heavy lines are guides to the eye.

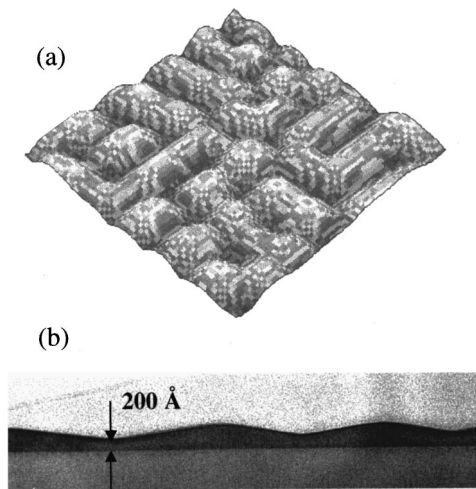


FIG. 9. (a) $2 \times 2 \mu\text{m}$ AFM image of 400 \AA $\text{Si}_{0.8}\text{Ge}_{0.2}$ film deposited at 630°C showing hut ridge morphology. (b) XTEM image of the same film showing the wetting layer and apparent ripple morphology.

observed wetting layer thickness of 200 \AA is significantly larger than the thickness, 60 \AA , at which island formation began, suggesting that the wetting layer does indeed grow at lower deposition temperature due to kinetic limitations on adatom diffusion and island coarsening. In the Discussion section we will estimate the relative contributions of the island lateral aspect ratio and the wetting layer growth on the overall effective stress.

Figure 10 shows another 400-\AA -thick film, deposited slightly warmer, at 642°C , where the surface is still composed of elongated hut ridges. However, with this small increase in temperature, at 400 \AA deposited thickness the early stages of dome cluster formation are observed. Thus, even in a situation where adatom diffusion is limited, the essential sequence of morphological transitions still occurs, albeit in a highly constrained fashion. Figure 10 also shows that where the $[201]$ and $[311]$ facets are forming, penetration through the wetting layer is taking place in the form deep grooves between the ridges. This is supported by AFM topographic images as well.

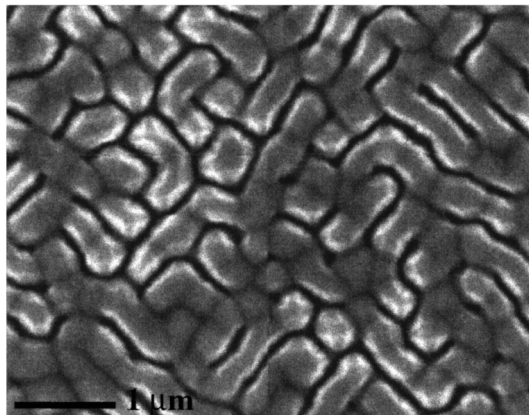


FIG. 10. Plan view SEM image showing incipient dome cluster formation in a 400-\AA -thick $\text{Si}_{0.8}\text{Ge}_{0.2}$ film deposited at 642°C .

COMPOSITION UNIFORMITY

The uniformity of the Si:Ge composition within the islands was investigated using energy dispersive spectroscopic (EDS) analysis of characteristic x ray generated in the sample. The sample was probed using an HB-501 dedicated scanning transmission electron microscope (STEM) operating at 100 kV . The probe was configured in the high current mode giving an $\sim 1.2\text{-nm}$ -diameter probe with a current of 1.0 nA . The samples were aligned so that the (001) growth direction was perpendicular to both the incident beam direction and the EDS detector port. The samples were tilted $\sim 10^\circ$ off the $[110]$ zone axis of the cross-section samples toward the $[1-10]$ direction to give an effective 30° take off angle for the characteristic x rays. Both simple intensity line scans and fully processed quantitative analyses were performed. For the quantitative analysis, reference spectra and k factors were obtained from the sample itself by recording and averaging spectra from the center of the SiGe islands and assuming this composition was equal to the deposited composition. Thus, the absolute calibration of the composition scale may be slightly off but relative changes are accurately measured.

Data were obtained from $\text{Si}_{0.8}\text{Ge}_{0.2}$ samples grown to three different thicknesses: a 275 \AA film deposited at 755°C that contains only dome clusters [see Fig. 5(b)], a 170 \AA film deposited at 755°C that exhibits a mixture of huts and domes, and a 400 \AA film deposited at 630°C that exhibits hut ridges and a thick metastable wetting layer (see Fig. 9). Both the line scans and the full quantitative analysis show a constant Si/Ge ratio in both the growth direction and parallel to the (001) planes, i.e., we do not detect significant compositional inhomogeneities within our films.

DISCUSSION

We have shown, through a combination of real time stress measurement during MBE growth and *ex situ* microscopy, that low strain $\text{Si}_{1-x}\text{Ge}_x$ alloys ($x_{\text{Ge}} = 0.2-0.35$, $\epsilon_{\text{coh}} = 0.008-0.014$) undergo a sequence of strain driven morphological transitions that qualitatively mirror those observed in Ge/Si(001) heteroepitaxy. In particular, we find that growth proceeds first as a fully strained 2D layer, followed by nucleation of discrete islands on top of the 2D layer, i.e., a Stranski-Krastanov-like transition. These islands stabilize as $[501]$ -faceted pyramids (hut clusters), which later transform into dome clusters bound by $[201]$ and $[311]$ facets. Further deposition eventually results in the introduction of dislocations into the islands. In order to observe these transitions unambiguously at low strain, the deposition temperature must be high enough so that the adatom diffusion length exceeds the length scale imposed by the energetics. In what follows, we discuss some important quantitative aspects of low-strain island formation.

Figure 6 explicitly demonstrates how the absolute strain affects the kinetics of roughening transitions. Low strain island formation is preceded by a much thicker wetting layer than is observed for Ge/Si(001), where the wetting layer thickness is consistently observed to be between 3 and 4 ml over a rather broad range of deposition conditions, suggesting that 3–4 ml represents an equilibrium wetting layer thickness for this system. However, for the alloys, even at

high deposition temperature, it is likely that the observed wetting layer thickness is kinetically established. For $x_{\text{Ge}} = 0.2$ deposited at 755°C and 0.1 \AA/s , the wetting layer thickness h_{wl} is approximately 18 ml, while for $x_{\text{Ge}} = 0.2$ deposited at 630°C and 0.1 \AA/s , h_{wl} is approximately 38 ml. For $x_{\text{Ge}} = 0.35$ deposited at 680°C and 0.13 \AA/s , h_{wl} is approximately 16 ml. We find that the wetting layer is slowly consumed during subsequent deposition and hut cluster formation at 755°C , but the rate of consumption has not been established, and we do not know whether some thin equilibrium wetting layer is still retained.

While increasing the Ge fraction from 0.2 to 0.35 does not drastically decrease the wetting layer thickness, we do observe from the MOSS data in Fig. 6 that the transition from planar to stable hut clusters occurs over a much narrower thickness range—only 4 \AA for $x_{\text{Ge}} = 0.35$ compared to a 40 \AA transition region for $x_{\text{Ge}} = 0.2$. In fact, with the interesting exception of the wetting layer, all the subsequent morphological regimes occur over thickness ranges that are severely reduced at $x_{\text{Ge}} = 0.35$ relative to those for $x_{\text{Ge}} = 0.2$, due to the increase in the strain energy density ($\propto \varepsilon_{\text{coh}}^2$). As mentioned earlier, the equivalent series of transitions for pure Ge deposition on Si(001) occur within the first 15 ml of deposition.

The thermodynamics of coherent island formation imposes a natural length scale $= \Delta\Gamma/M\varepsilon_{\text{coh}}^2$, as mentioned in the Introduction. However, the two stress curves in Fig. 6 cannot be collapsed exactly upon one another simply by scaling as $\varepsilon_{\text{coh}}^{-2}$. This is primarily the result of kinetic effects, since island formation during deposition is occurring away from equilibrium. A complete theory that would force the two stress curves to collapse would require full accounting for the deposition rate and temperature, and all kinetic pathways associated with the various morphological transitions, including the nucleation modes for huts, domes, and dislocations, the elastic interactions between neighboring islands and between islands and adatoms, and coarsening. Individual elements of this problem have been addressed in varying levels of detail, but a comprehensive theory has not yet been developed.

Previous experiments in Si-rich $\text{Si}_{1-x}\text{Ge}_x$ alloys have suggested that roughening occurs in the form of a continuous ripple, rather than as discrete islands that are observed at higher strains.⁵ Further there exist competing theories of strain driven roughening, by continuous ripple formation, e.g., the Asaro-Tiller-Grinfeld instability theory,^{6,7} vs theories of discrete island formation.⁴ This has led to some confusion on the effect of the absolute magnitude of the mismatch strain on the fundamental roughening process. However, our data clearly indicates that in the $\text{Si}_{1-x}\text{Ge}_x/\text{Si}$ system, for $x \geq 0.2$, there is no fundamental difference in roughening behavior as a function of strain. In particular, comparison of Fig. 9 for the morphology of our $\text{Si}_{0.8}\text{Ge}_{0.2}$ films grown at 630°C with those for similar growths in Ref. 5, combined with our 755°C data, demonstrates that the apparent ripple is simply a kinetically constrained hut cluster morphology. The limited adatom diffusion length at 630°C relative to the intrinsic length scale at low strain causes coalescence of islands at an early stage (i.e., at approximately 135 \AA film thickness, according to Fig. 8). Coalescence promotes elongated islands and the growth of the underlying

wetting layer, which leads to the ripplelike appearance in cross section.

On the other hand, formation of a ripplelike structure at very early stages of low strain roughening may occur as a kinetic pathway for the nucleation of discrete hut clusters [Fig. (4)]. This process has been observed by Dorsch *et al.*³¹ We observe a similar intermediate roughening stage [see Fig. 4(b)] wherein a disorganized ripple morphology appears to serve as a precursor to discrete hut clusters. The “facet angle” of the ripples continuously increases until the [501] facet locks in. In an apparently related phenomenon at higher Ge content and strain ($x_{\text{Ge}} = 0.5$), Chen *et al.* have observed discrete islands whose facet angle also continuously increases until stabilizing at [501].³² It is not known for pure Ge on Si(001), where the driving force for island formation is very large, and the length scales correspondingly are very small, whether islands nucleate “directly” as hut clusters, or first pass briefly through some intermediate state analogous to those observed here and by others in experiments at low strain.

Our MOSS data provide a quantitative measure of the degree of stress relaxation associated with the compact hut cluster morphology. Steinfort *et al.* recently reported x-ray measurements of the vertical strain distribution in Ge hut clusters.³³ Integrating their strain distribution gives a 15% effective relaxation, less than the $20 \pm 2\%$ value for $\text{Si}_{0.8}\text{Ge}_{0.2}$ huts reported here. We have grown Ge on Si(001) under conditions similar to Ref. 33 while measuring the curvature in real time,¹¹ and we obtain an effective relaxation for Ge huts that is consistent with our alloy measurements, although the error bars for this measurement are somewhat larger. Due to this, we cannot say definitively that the strain distributions in $\text{Si}_{0.8}\text{Ge}_{0.2}$ huts are identical to those in pure Ge huts. Continuum elastic analysis of the bulk strain fields predicts that the strain distribution and effective relaxation only depends on island shape, and not on the island size or the absolute mismatch strain.²⁶ However, at relatively small island volumes, as is the case in pure Ge huts, the elastic effects of the island edges, which act as discontinuities in the surface stress, may become important.^{34,35}

The dome cluster morphology relieves considerably more stress than the hut clusters. The instantaneous stress, proportional to dk/dh_f , is only $0.33\sigma_{\text{coh}}$ in the dome regime. The average stress, proportional to κ/h_f , is $0.5\sigma_{\text{coh}}$. Despite the large stress concentration at the perimeter of the domes, they retain fully coherent interfaces according to plan view TEM. Careful inspection of the contact perimeter between the dome clusters and the Si substrate reveals that a trench in the substrate forms around the island.¹⁸ This acts to reduce the local elastic energy by reducing the effective contact angle, and by rejecting substrate material from the high strain region. Trenches have also been observed in the case of pure Ge domes on Si(001).³⁶ It is only when copious impingement of dome clusters occurs at high deposition thickness that dislocations are able to nucleate.

The stress relaxation for $\text{Si}_{0.8}\text{Ge}_{0.2}$ deposition at 630°C is less than that at 755°C partly because the islands typically have rectangular bases, with lateral aspect ratios in the range 1:1–1:3. We can estimate the effective stress for an array of 1:n sized islands, sketched in Fig. 11 for the case $n = 2$. Across the narrow dimension of the islands, the amount of

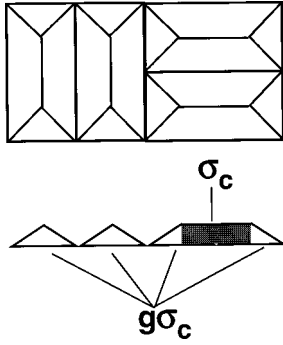


FIG. 11. A schematic illustration used to estimate the degree of effective stress relaxation in hut ridges.

stress relaxation is nearly the same as for compact islands, i.e., equal to $g\sigma_{\text{coh}}$, where g is the fractional relaxation. Across the long dimension of the islands, we assume for simplicity that the end sections of the islands also exhibit the effective stress of compact islands, while the interior section, shown shaded in Fig. 11, is at the full coherency stress (this will tend to overestimate the average strain in the elongated island). The volume of the interior section is $1.5(n-1)V_{\text{compact}}$, where V_{compact} is the volume of a square based pyramid. The overall effective stress is then given by

$$\sigma_{\text{eff}} = \left[\frac{2g(n+1) + 3(n-1)}{5n-1} \right] \sigma_{\text{coh}}. \quad (5)$$

For $n=2$ and $g=0.78$, we get $\sigma_{\text{eff}} \approx 0.85\sigma_{\text{coh}}$. We measure $\sigma_{\text{eff}}=0.9\sigma_{\text{coh}}$ in Fig. 9, suggesting that wetting layer growth also contributes to the measured effective stress.

This can be used to provide a lower bound on the rate of growth of the wetting layer. Using Eq. (2), and taking $\sigma_{\text{eff}}=0.9\sigma_c$, and $g_{\text{isl}}=0.85$ for the 1×2 island shape, we obtain $\Phi_w > 0.23\Phi$, where Φ_w is the effective deposition rate into the wetting layer and Φ is the actual deposition rate. Thus, at least 20% of the arriving adatoms incorporate into the energetically unfavorable wetting layer, kinetically forced there due to insufficient surface mobility. At higher temperature, e.g., deposition of $\text{Si}_{0.8}\text{Ge}_{0.2}$ at 755°C , huts clusters are able to assume the ideal compact shape and the wetting layer thickness is constant or slowly decreases.

The lack of compositional nonuniformity within our islands is surprising since differing attachment biases for Si and Ge adatoms as a function of local surface strain are expected on theoretical grounds.^{37,38} While bulk lateral composition modulation is frequently observed in III-V systems,³⁹ there is scant evidence for this effect in coherently strained SiGe islands.⁴⁰ The complex evolution of a discrete island (including coarsening, coalescence, and shape transitions) may effectively smear out internal compositional nonuniformity.

Finally we note that a clear benefit of examining dynamic processes in coherent island evolution at low strain is that the

various morphological regimes are greatly extended in thickness. This permits detailed examination of processes occurring within each regime that are difficult to obtain, for example, in pure Ge growth on Si, where transitions occur within a monolayer or two, and much of the interesting island evolution is complete within 15 monolayers of growth. We have exploited this fact to study in detail the hut-to-dome transition, where we show that elastic interactions between huts dramatically affects the energetics of the transition.¹⁶ We have also shown that elastic interactions cause accelerated coarsening and lateral ordering of hut clusters.¹⁷ These observations are further facilitated by the larger lateral length scales associated with low strain island formation, which permit use of *optical* scattering probes,^{15,17} and which reduce the resolution requirements on scanning force and electron probes.

CONCLUSIONS

Real time curvature measurement during SiGe MBE growth has been shown to be very useful in the study of coherent islanding transitions. The real time data immediately indicate when morphological transitions are occurring. This guides our use of *ex situ* imaging, allowing for efficient identification of the different morphological regimes of growth as a function of coherency strain and deposition temperature. We find that growth of low strain $\text{Si}_{1-x}\text{Ge}_x$ alloys on Si(001) exhibits a qualitatively identical sequence of roughening transitions to pure Ge on Si(001). The quantitative differences arise from the dependence of the fundamental length scale that is established by the competition between surface energy and bulk strain energy. Furthermore, adatom diffusion kinetics play a critical role in controlling the detailed island morphology. At low strain, the lateral length scales are large, and the deposition temperature must then also be large in order to observe the true nature of the island transitions. The kinetic pathways for these transitions can be examined in detail since the transitions occur over a broader range of film thickness than at high strain. While it must be acknowledged that the kinetic pathways at higher strain may differ from those at low strain, we nonetheless gain significant insight into the energetics and kinetics of islanding transformations that benefit our understanding of morphological evolution at high strain.

ACKNOWLEDGMENTS

Our thanks to John Hunter for his assistance with the MBE growths, Bob Cammarata for his insights, and Bonnie McKenzie for her excellent SEM work. L.B.F. acknowledges the MRSEC program at Brown University funded by the National Science Foundation under Award No. DMR-9632524. Sandia is a multiprogram laboratory operated by Sandia Corporation, a Lockheed Martin Company, for the United States Department of Energy under Contract No. DE-AC04-94AL85000.

- ¹Y.-W. Mo, D. E. Savage, B. S. Swartzentruber, and M. G. Lagally, *Phys. Rev. Lett.* **65**, 1020 (1990).
- ²D. J. Eaglesham and M. Cerullo, *Phys. Rev. Lett.* **64**, 1943 (1990).
- ³S. Guha, A. Madhukar, and K. C. Rajkumar, *Appl. Phys. Lett.* **57**, 2110 (1990).
- ⁴J. Tersoff and F. K. LeGoues, *Phys. Rev. Lett.* **72**, 3570 (1994).
- ⁵A. J. Pidduck, D. J. Robbins, A. G. Cullis, W. Y. Leong, and A. M. Pitt, *Thin Solid Films* **222**, 78 (1992).
- ⁶R. J. Asaro and W. A. Tiller, *Metall. Trans. A* **3**, 1789 (1972).
- ⁷M. A. Grinfeld, *Sov. Phys. Dokl.* **31**, 831 (1987).
- ⁸D. J. Srolovitz, *Acta Metall.* **37**, 621 (1989).
- ⁹B. J. Spencer, P. W. Voorhees, and S. H. Davis, *J. Appl. Phys.* **73**, 4955 (1993).
- ¹⁰J. A. Floro and E. Chason, in *Diagnostic Techniques for Semiconductor Materials Processing II*, edited by S. W. Pang, O. J. Glembocki, F. H. Pollak, F. G. Celli, and C. M. Sotomayor Torres, MRS Symposia Proceedings No. 406 (Materials Research Society, Pittsburgh, 1996), p. 491.
- ¹¹J. A. Floro, E. Chason, S. R. Lee, R. D. Twisten, R. Q. Hwang, and L. B. Freund, *J. Electron. Mater.* **26**, 983 (1997).
- ¹²Paul A. Flinn, Donald S. Gardner, and William D. Nix, *IEEE Trans. Electron Devices* **ED-34**, 689 (1987).
- ¹³R. C. Cammarata, *Prog. Surf. Sci.* **46**, 1 (1994).
- ¹⁴G. G. Stoney, *Proc. R. Soc. London, Ser. A* **82**, 172 (1909).
- ¹⁵Eric Chason, Michael B. Sinclair, Jerry A. Floro, John Hunter, and Robert Q. Hwang, *Appl. Phys. Lett.* **72**, 3276 (1998).
- ¹⁶J. A. Floro, G. A. Lucadamo, E. Chason, L. B. Freund, M. Sinclair, R. D. Twisten, and R. Q. Hwang, *Phys. Rev. Lett.* **80**, 4717 (1998).
- ¹⁷J. A. Floro, E. Chason, M. Sinclair, L. B. Freund, and G. A. Lucadamo, *Appl. Phys. Lett.* **73**, 951 (1998).
- ¹⁸J. A. Floro, E. Chason, R. D. Twisten, R. Q. Hwang, and L. B. Freund, *Phys. Rev. Lett.* **79**, 3946 (1997).
- ¹⁹J. A. Floro and E. Chason, *Appl. Phys. Lett.* **69**, 3830 (1996).
- ²⁰C. Ratsch, P. Smilauer, D. D. Vvedensky, and A. Zangwill, *J. Phys. I* **6**, 575 (1996).
- ²¹Harvey T. Dobbs, Dimitri Vvedensky, Andrew Zangwill, Jonal Johansson, Niclas Carlsson, and Werner Seifort, *Phys. Rev. Lett.* **79**, 897 (1997).
- ²²J. W. Matthews and A. E. Blakeslee, *J. Cryst. Growth* **27**, 118 (1974).
- ²³D. E. Jesson, K. M. Chen, S. J. Pennycook, T. Thundat, and R. J. Warmack, *Phys. Rev. Lett.* **77**, 1330 (1996).
- ²⁴M. Hammar, F. K. LeGoues, J. Tersoff, M. C. Reuter, and R. M. Tromp, *Surf. Sci.* **349**, 129 (1996).
- ²⁵M. Tomitori, K. Watanabe, M. Kobayashi, and O. Nishikawa, *Appl. Surf. Sci.* **76/77**, 322 (1994).
- ²⁶H. T. Johnson and L. B. Freund, *J. Appl. Phys.* **81**, 6081 (1997).
- ²⁷F. Jonsdottir and L. B. Freund, in *Thin Films—Structure and Morphology*, edited by S. Moss, D. Ila, R. C. Cammarata, E. H. Chason, T. L. Einstein, and E. D. Williams, MRS Symposia Proceedings No. 441 (Materials Research Society, Pittsburgh, 1997), p. 495.
- ²⁸Gilberto Medeiros-Ribeiro, Alexander M. Bratkovski, Theodore I. Kamins, Douglas A. A. Ohlberg, and R. Stanley Williams, *Science* **279**, 353 (1998).
- ²⁹F. M. Ross, J. Tersoff, and R. M. Tromp, *Phys. Rev. Lett.* **80**, 984 (1998).
- ³⁰Mohan Krishnamurthy, J. S. Drucker, and J. A. Venables, *J. Appl. Phys.* **69**, 6461 (1991).
- ³¹W. Dorsch, B. Steiner, M. Albrecht, H. P. Strunk, H. Wawra, and G. Wagner, *J. Cryst. Growth* **183**, 305 (1998).
- ³²K. M. Chen, D. E. Jesson, S. J. Pennycook, T. Thundat, and R. J. Warmack, *Phys. Rev. B* **56**, R1700 (1997).
- ³³A. J. Steinfert, P. M. L. O. Scholte, A. Ettema, F. Tuinstra, M. Nielsen, E. Landenmark, D.-M. Smilgies, R. Feidenhans'l, G. Alkenberg, L. Seehofer, and R. L. Johnson, *Phys. Rev. Lett.* **77**, 2009 (1996).
- ³⁴V. A. Shchukin, N. N. Ledentsov, P. S. Kop'ev, and D. Bimberg, *Phys. Rev. Lett.* **75**, 2968 (1995).
- ³⁵J. Tersoff, *Phys. Rev. Lett.* **79**, 4934 (1997).
- ³⁶T. I. Kamins, E. C. Carr, R. S. Williams, and S. J. Rosner, *J. Appl. Phys.* **81**, 211 (1997).
- ³⁷J. E. Guyer and P. W. Voorhees, *Phys. Rev. Lett.* **74**, 4031 (1995).
- ³⁸P. Venezuela, J. Tersoff, J. A. Floro, E. Chason, D. M. Follstaedt, Feng Liu, and M. G. Lagally (unpublished).
- ³⁹J. Mirecki-Millunchik, R. D. Twisten, S. R. Lee, D. M. Follstaedt, E. D. Jones, S. P. Ahrenkiel, Y. Zhang, H. M. Cheong, and A. Mascarenhas, *MRS Bull.* **22**, 38 (1997).
- ⁴⁰T. Walther, C. J. Humphreys, and A. G. Cullis, *Appl. Phys. Lett.* **71**, 809 (1997).